Optical and Quantum Electronics (2023) 55:1043
https://doi.org/10.1007/s11082-023-05329-z

Graphene based SRR with quadrupole mode loaded on two port antenna with high isolation and polarization diversity for THz applications

Anubhav Kumar[1] · **Divya Saxena**[2]

Received: 28 June 2023 / Accepted: 25 August 2023 / Published online: 21 September 2023

Abstract
In this paper, graphene based SRR loaded on a two-port antenna with high isolation and polarization diversity is used for THz applications. The size of the two-port antenna is compact and two microstrip-fed radiators are placed orthogonally to achieve the polarization diversity. The defective ground and stub are implemented to achieve impedance matching and isolation enhancement. The SRR is loaded on the ground which is based on the quadrupole mode of the electric field and perturbs the surface waves which creates null and weak electric field between antenna elements. The SRR improves the isolation up to 17.23 dB where the distance of edges of the antenna is only 0.15 λ. The SiO_2 substrate-based two-port antenna works from 4.9 to 6.3 THz with maximum isolation of 42.3 dB which can be tunable with different chemical potentials applied to SRR.

Keywords Two-port antenna · Quadrupole mode (QM) · Graphene antenna · Isolation enhancement · SRR

1 Introduction

THz frequency band which has immense bandwidth potential and can be a better option for 6G communication which has considering the demand of high channel capacity and bandwidth. However, the THz band can be used for short and indoor communication due to high transmission and molecular loss where THz band has high absorption instead of GHz frequency (Akyildiz et al. 2018).THz frequency band from 0.1 to 10 THz can be used in different applications such as vehicular, sensing, space, WBAN, biomedical, and short-range (Okan 2021; Woolard et al. 2005; Hwu et al. 2013; Rubani et al. 2020; Prabhu

✉ Anubhav Kumar
rajput.anubhav@gmail.com

Divya Saxena
drdivyasaxena06@gmail.com

[1] Department of Electronics and Communication Engineering, Raj Kumar Goel Institute of Technology and Management, Ghaziabad, Uttar Pradesh 201003, India

[2] Department of Applied Science and Humanities, ABES Engineering College, Ghaziabad, Uttar Pradesh 201009, India

and Malarvizhi 2022; Kumar and Saxena 2020). The antenna is an important part of wireless communication that can transmit and receive the EM waves. As per new requirement single-element antenna is not a suitable choice for THz communication therefor required the multi-element antenna or MIMO antenna which improve the performance in a multipath environment. The correlation between antenna elements is the important parameter and required a minimum distance of half wavelength to uncorrelated the antenna from each other. The MIMO antenna requires minimum space in the antenna elements to make a compact antenna but it increases the coupling and correlation and affects the antenna parameters. The many decoupling technologies introduced in the literature minimize the antenna size and improve the isolation of defected ground (Saxena et al. 2020; Prabhu and Malarvizhi 2022), distance/unconnected ground (Keshwala 2021; Vasu Babu and Das 2022; Okan 2021; Rubani et al. 2020), tunable decoupling (Maurya et al. 2023; Singh and Varshney 2023) and parasitic strip (Vijayalakshmi et al. 2021). In (Saxena et al. 2020), an elliptical-shaped radiator with microstrip fed and the partial ground is implemented on RT5880 substrate where the size of the antenna is large compared to recent work, and the defective ground is used to increase the port isolation. In (Keshwala 2021), the square-shaped radiator is changed to sinusoidal which improves the electrical length and improve the impedance bandwidth. The partial ground of the antenna is unconnected and helps to enhance the port isolation. In (Maurya et al. 2023), the microstrip fed radiator and ring slot are loaded on the ground to improve the impedance matching (IM) and is used to design a tunable two-port antenna where the tuning decoupling network based on graphene is used to suppress the coupling current. In (Vasu Babu and Das 2022), a tree-shaped radiator implemented on polyimide with the partial ground is used where the partial ground and tree-shaped radiator are used to improve the impedance matching and unconnected ground which support the uncorrelated antenna response. In (Okan 2021), the tapered-shaped feed and modified radiator are used to improve the impedance bandwidth where the radiator is placed orthogonally and unconnected ground support to suppress the coupling current. In (Rubani et al. 2020), the electric length of the radiator is increased by a four-rectangular radiator where the isolation is improved with a quarter wavelength distance of the antenna which weakens the coupling current. In (Prabhu and Malarvizhi 2022), the radiator is modified in the Koch fractal-shaped to improve the IM of the antenna where the defective ground is used to weaken the surface current. In (Vijayalakshmi et al. 2021), the electric length of the antenna is modified with a series-placed patch and parasitic strip to eliminate and perturbs the surface current which improves the port isolation. In (Das et al. 2022), a modified rectangular radiator with a loaded graphene strip for tuning and a T-shaped stub is used to improve the isolation where the graphene also improves the port isolation. In (Singh and Varshney 2023), a single radiator is used to design the two-port antenna where the graphene and multiple slots in the radiator are used to eliminate the coupling current which reduces the correlation between antenna. In (Aghamohammadi et al. 2022), the modified rectangular-shaped radiator placed in the 180° rotated and metamaterials are used to diminish the surface current without affected the resonant frequency in THz bands. In (Kiani et al. 2022a), polarization reconfigurable antenna is discussed with graphene in leaf-shaped patch antenna without affected the physical shape. In (Kiani et al. 2022b), the graphen and SIW based antenna is designed on silicon dioxide substrate with size miniaturized and reconfigurable properties. In (Kiani et al. 2023), slot based microstrip pathe antenna is discussed with graphene and gold conductor where the slot are based on gold conductor and responsible for polarization change from right-hand to left-hand circular polarization. In (Ali et al. 2023), monopole antenna is designed with microstrip-fed where the graphene is accomplished in the slot and produces the filtering characteristics

with tunable behaviour. In (Vishwanath et al. 2023), graphene strips are utilized in the slot and dielectric resonator based single element antenna where the bandwidth and isolation can be improved with variation of electrical characteristics of graphene. In (Nickpay et al. 2023a), four split ring resonator and metal ring are used to triple-band absorber and frequency can be shift with change in chemical voltage on grapheme. In (Nickpay et al. 2023b), fan-shaped and graphene based absorber is designed for quad band THz application which can be controlled by the chemical potential on graphene. In (Nickpay et al. 2022a), patch with split ring resonator are used to design the triple band absorber based on the metamaterial characteristics which can be used for Refractive Index (RI) sensor in THz bands. In (Nickpay et al. 2022b), I-shaped and two u-shaped graphene conductor are placed for triple band absorber where the double band is responsible for u-shaped graphene and single band is based on I-shaped graphee triple band can be controlled and shifted with chemical potential on graphene. In (Nickpay et al. 2022d), modified split ring resonator is used to designed absorber where the frequency can be tuned with applied bias voltage on graphene. In (Nickpay et al. 2021), the structure of the graphene strip is based on two-rectangular with cross shaped strip for wider bandwidth as a absorber, which is insensitive to polarization and can be applicable in THz band. In (Nickpay et al. 2022c), absorber based on graphene is designed for THz band and can be controlled by external potential applied on graphene. In the recent work, many decoupling technologies are discussed with the unconnected ground, the distance between the antenna, and defected ground where the graphene-based tuning model which increases the isolation and attractive choice in THz applications. In this approach, a tuning graphene is used to modify the isolation and |S11| of the two-port antenna where novel SRR is loaded based on graphene substrate in the two-port antenna. The SRR-loaded two-port antenna novelty and technical considerations are discussed below.

1. The Two-port antenna is implemented on Silicon dioxide (SiO_2) where the size of the antenna is only $30 \times 30\ \mu m^2$.
2. The distance from edges of the antenna elements is only $0.15\lambda_0$ which is small compared to conventional distance ($0.5\lambda_0$).
3. The diagonal stub and defected ground is used to improve the impedance matching and improve the port isolation of the antenna.
4. The SRR based graphene material which has the tuning characteristics of the antenna parameters is placed on the ground. The SRR introduced the quadrupole mode of the electric field and perturbs the surface waves. The SRR occurred the high electric filed which weaken and null the electric field between the antenna and improve the port isolation upto 17.23 dB.
5. The antenna element position is orthogonal which is help to achieve the polarization diversity.
6. The decoupling technology of the MIMO antenna is simple, novel with connected ground which reduces the design complexity.

2 Design of the two-port antenna

The two-port antenna is used to design for THz application and implemented on the Silicon dioxide as a substrate where the conducting element used is gold whose thickness is 35 nm as illustrated in Fig. 1a The graphene-based SRR loaded on the two-port antenna for tuning

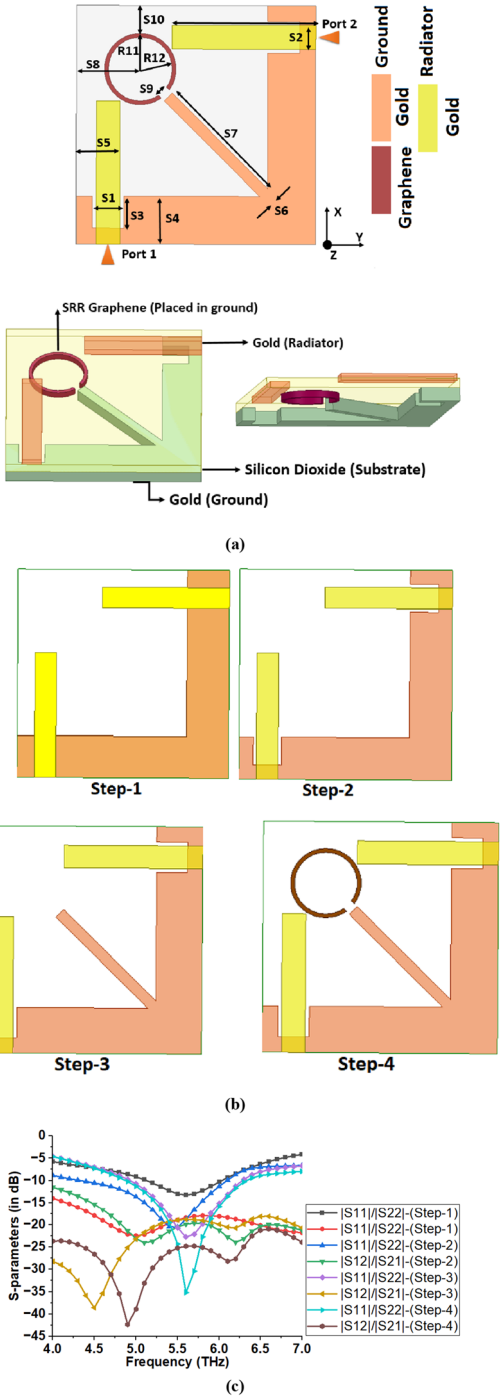

Fig. 1 Two-port antenna **a** Antenna view (All dimensions in μm—S1 = 4, S3 = 4, S5 = 5.5, S7 = 12, S9 = 1, R11 = 4.5, S2 = 3, S4 = 6, S6 = 1, S8 = 8, S10 = 3.5, R12 = 4, S13 = 18). **b** Antenna steps. **c** S-parameters. **d** Electric field variation. **e** Effect of SRR. **f** Optimization of SRR

performance and improve the port isolation which thickness (Δ) is 0.34. The microstrip fed

Fig. 1 (continued)

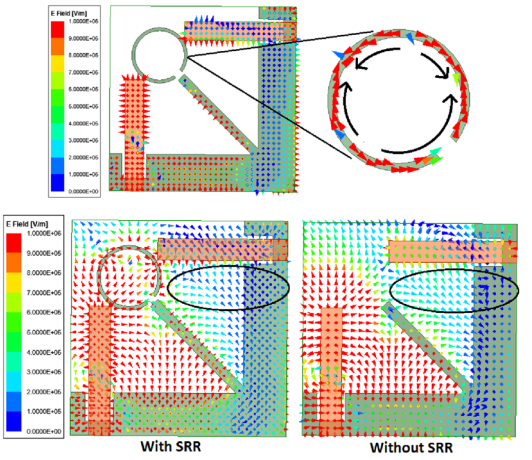

(d)

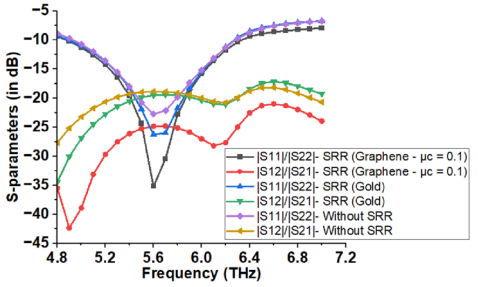

(e)

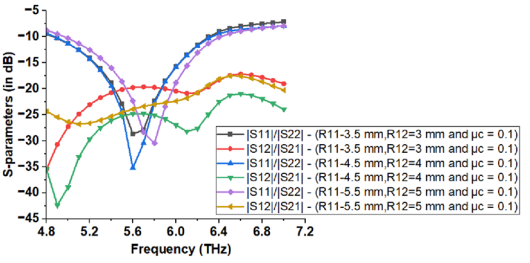

(f)

is used as a radiator whose width is determined from Eqs. (1) to (3).

$$\text{If } \frac{S_2}{t} > 1 \text{ then} \tag{1}$$

$$\varepsilon_{eff} = \frac{\varepsilon_{r+1}}{2} + \frac{\varepsilon_r - 1}{2}\left[1 + 12\frac{t}{S_2}\right]^{-\frac{1}{2}} \tag{2}$$

$$Z_0 = \frac{120\pi}{\sqrt{\varepsilon_{eff}}\left[\frac{S_2}{t} + 1.393 + (2/3)\ln\left(\frac{S_2}{t} + 1.444\right)\right]} \tag{3}$$

The determined value of the width is 3 µm when the substrate thickness (t) is 1.5 µm and Zo is 50 Ω where S2 is the width of microstrip line, ε_{eff} and ε_r are the effective dielectric constant and dielectric constant (Balanis 2015). The evolution steps of the two-port antenna are illustrated in Fig. 1b where the s-parameters are depicted in the Fig. 1c. In step-1, two microstrip-fed radiators with a length of 18 µm and width of 3 µm are used and placed orthogonally to achieve polarization diversity. The partial ground is used with a length of 6 µm to achieve impedance matching. The |S11| of the antenna is obtain from 5.15 THz to 6 THz with isolation above 17 dB. In step-2, the rectangular slot is introduced on the ground behind the feed line which improves the impedance matching, and the bandwidth of the two-port antenna is enhanced. The |S11| of the antenna is obtain from 4.4 THz to 6.1 THz with isolation above 14 dB. In Step-3, the diagonal stub is accomplished in the ground to increase the isolation which perturbs the surface current and improves the ground length. The |S11| of the antenna is obtain from 4.4 THz to 6.1 THz with isolation above 14 dB. In step-4, a graphene material-based Split Ring Resonator (SRR) is introduced in the ground at a chemical potential of 0.1 eV which generates a quadrupole mode of the electric field which is represented in Fig. 1d where the four different directions of electric field movement are visible in SRR. The arrow in back color represent the direction of the electric field. The SRR occurred the high electric field and perturbs the surface waves as well produce weaken and null electric field represent in the black circle in Fig. 1d which eliminates the coupling and improves the port isolation up to 17.23 dB. The SRR effect is illustrated in the Fig. 1e, where the where the enhancement of isolation is much higher with graphene compare to SRR with metal and without SRR and which shows that the graphene with quadrupole mode perfectly diminish the surface wave in between antenna element. The optimization steps of the SRR with different radiaus of the R11 and R12 with step size of 1 µm is represented in the Fig. 1f where the optimized value is achieved of the s-parameters of radius R11 and R12 is 4.5 µm and 4 *µm* respectively which enhances the 17.23 dB of isolation.

3 Graphene loaded on two-port antenna

The graphene is used in SRR and loaded on the two-port antenna with electrical parameters, such as relaxation time (τ) = 2 ps, Chemical potential (µc) = 0.1 eV and temperature (T) = 300 K, scattering rate (Γ), reduced Plank's constant ($\hbar$), electronic charge (e). The dielectric coefficient of the silicon dioxide is 3.9 and loss tangent is 0.0006 are used (Maurya et al. 2023). The surface conductivity (σ) is determined from the Intraband conductivity and Interband conductivity by Kubo's formula from Eqs. (4)–(6) (Kaipa et al. 2012; Qi et al. 2019; Maurya et al. 2023;). The conductivity of the graphene can be varied from the applied chemical potential and the permittivity is determined from Eq. (7), where Δ is the thickness of the graphene and ε_0 is the permittivity of free space. The determined value of the Intraband conductivity and the total conductivity in real and imaginary form is illustrated in Fig. 2a and Interband conductivity is represent in the Fig. 2b from 0.2 to 10 THz. The determined permittivity of the grapheme is illustrated in Fig. 2c in real and imaginary value which is extracted from Eq. (7).

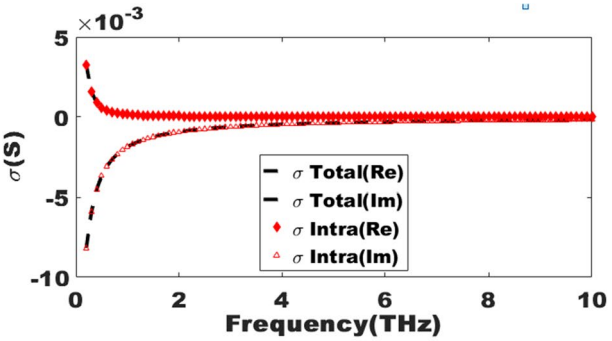

(a)

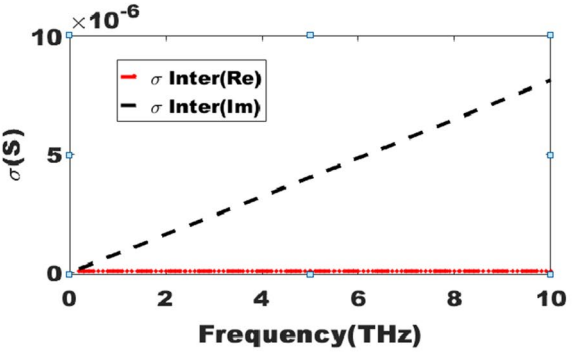

(b)

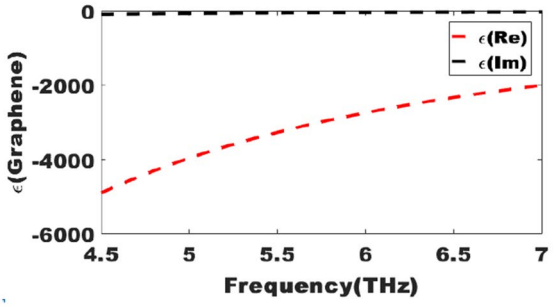

(c)

Fig. 2 Graphene analysis. **a** Intraband and total conductivity. **b** Interband conductivity. **c** Permittivity

$$\sigma_{intraband}(w,\mu_c,\Gamma,\mathrm{T}) = -j\frac{e^2 k_B T}{\pi\hbar^2(w-j\Gamma)}\left[\frac{\mu_c}{k_B T} + 2ln\left(e^{\frac{-\mu_c}{k_B T}}+1\right)\right] \tag{4}$$

$$\sigma_{interband}(w,\mu_c,\Gamma,\mathrm{T}) = -j\frac{e^2}{4\pi\hbar} In\left[\frac{2|\mu_c| - (w-j\Gamma)\hbar}{2|\mu_c| + (w-j\Gamma)\hbar}\right] \tag{5}$$

$$\sigma_{Graphene} = \sigma_{Total} = \sigma_{intraband} + \sigma_{interband} \tag{6}$$

$$\varepsilon_{Graphene} = 1 - \frac{j\sigma_{Graphene}}{w\varepsilon_0\Delta} \tag{7}$$

The s-parameters of the two-port antenna are determined at the different chemical potentials to evaluate the effectiveness of the tuning behaviour of the graphene. The s-parameters at the different chemical potentials of 0.1 eV (Optimized), 0.15 eV, 0.2 eV, 0.25 eV, and 0.3 eV are illustrated in Fig. 3a where the resonance frequency of the two-port antenna is shifted to a higher frequency, and isolation is decreased when the chemical potential is increased. The gain and efficiency at different chemical potentials are illustrated in Fig. 3b, c and detailed analyses are represented in the Table 1. The optimized value used for chemical potential is 0.1 eV where the |S11| varied from 4.9 to 6.3 THz and isolation of 24.8 dB to 42.3 dB is achieved. The results illustrated the chemical potential of graphene used in SRR effectively tune the s-parameters of the two-port antenna. The conductivity and Fermi

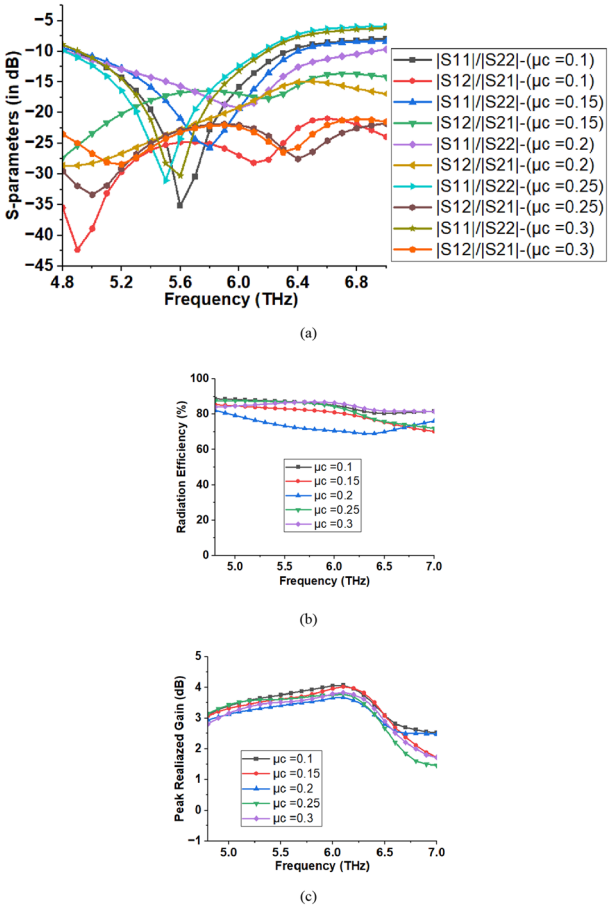

Fig. 3 Analysis of SRR graphene in two-port antenna. **a** S-parameters. **b** Efficiency. **c** Gain

Table 1 Analysis of graphene on two-port antenna at different Chemical potential (μ_c)

Chemical potential (μ_c) eV	|S11| in dB	Isolation (dB)	Gain (dB)	Efficiency (%)
0.1	4.9 to 6.3	24.8 to 42.3	3.27 to 4	81.5 to 88.8
0.15	4.9 to 6.4	15.5 to 25.4	3.2 to 4	76.8 to 85
0.2	4.8 to 6.9	15 to 28.6	2.5 to 3.68	75 to 82
0.2.5	4.8 to 6.15	21.8 to 33.3	3.1 to 3.78	82 to 87
0.3	4.92 to 6.18	22 to 28.4	3 to 3.76	84 to 86

level of the graphene can be adjusted by using ion-gen with gold as electrode which is common in practice where the thickness of the ion-gen is small and this provides transparency and large carrier density in THz bands (Nickpay et al. 2023a, 2022a; Sorathiya et al. 2022; Wang et al. 2022). The electrical properties of the graphene is calculated by the Eqs. (4)–(7), and is inserted the real and imaginary values of set frequency dependency in HFSS. The surface impedance in the HFSS is defined from the ($z = 1/\sigma$) as a boundary condition for accurate results (Torabi et al. 2017; Gao et al. 2020; Dash and Patnaik 2021).

4 EC model analysis

The SRR-loaded two-port antenna is used to validate with the electronics circuit (EC) model where the lumped element of the EC model is determined from the QUCS software. The EC model and s-parameters are illustrated in Fig. 4a, b. The capacitance and inductance of both orthogonally placed microstrip fed are represented in the Ls1/Lr1 and Cs1/Cr1. The Ld, Cd, and Rd are demonstrating the decoupling of the two-port antenna. The Cs2/Cr2, Ls2/Lr2, and Rs2/Rr2 tank circuit demonstrate the single band operating frequency where the final value of the S-parameters is determined from the EC model and HFSS are represented in the Fig. 4b where the similar response is found which validate the proposed SRR loaded two-port antenna.

5 Results analysis of the SRR loaded two-port antenna

The SRR-loaded two-port antenna is implemented on the HFSS-19 for THz applications where the EC model is used to authenticate the S-parameters. The |S11| of the Two-port antenna is obtain from 4.9 to 6.3 THz and isolation of 24.8 dB to 42.3 dB where maximum isolation of 42.3 dB at the chemical potential of 0.1 eV is found as illustrated in Fig. 5a. The gain (dB) and efficiency (%) of the SRR-loaded two-port antenna are represented in Fig. 5b, c. The gain of the antenna obtain from 3.27 to 4 dB and the efficiency of the antenna achieved from 81.5 to 88.8% showing the efficient result in compact antenna and silicon dioxide substrate. The normalized radiation pattern of two-port antenna at 5.6 THz in xz ($\theta = all and \varphi = 0°$), xy ($\theta = 90° and \varphi = all$) and yz (($\theta = all and \varphi = 90°$),) direction are illustrated in the Fig. 5d–f where the results are omnidirectional and stable. MIMO characteristics of the antenna are evaluated by the ECC, DG, TARC, and CCL from Eqs. (8)–(12) which is calculated from the s-parameters and illustrated in Fig. 6. The Envelope

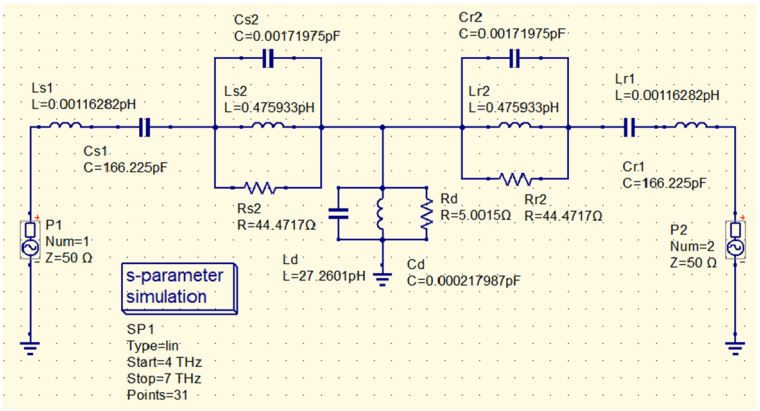

(a)

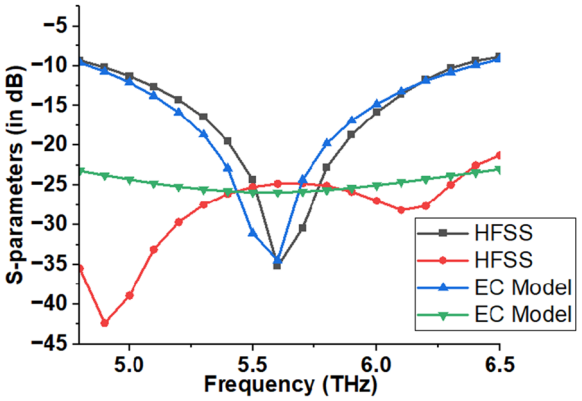

(b)

Fig. 4 EC model from QUCS. **a** EC model. **b** S-parameters

Correlation Coefficient (ECC) represents the coupling between the antenna where the 0 value is indicating a low correlation and low mutual coupling and the 1 value is indicating a high correlation and high mutual coupling. The ECC is determined from the s-parameters and calculated from the Eq. (8). The ECC of the antenna can effectively determine the how much antenna is independent and not affected by other antenna elements placed nearby. The upper rate of the ECC should be 0.5 where the SRR-loaded two-port antenna is below 0.002. The Diversity gain (DG) should be near 10 dB which represents the uncorrelated antenna whereas the SRR-loaded two-port antenna is close to 10 dB and shows the diversity characteristics of the antenna. The TARC is evaluated from the square root of the reflected to accept power and represent the efficiency and bandwidth of the antenna as illustrated in the Eq. (10) where |b| represent the reflected vector and |a| represent the excitation vector. TARC is represented in the figure and shows the minimum effect of the variation with different phase angles and calculated by Eq. (11) (Varshney et al. 2019) where the |S11| and |S12| are the reflection and transmission coefficient of the two-port antenna and θ is the input phase of feed. The Channel Capacity Loss (CCL) is determined

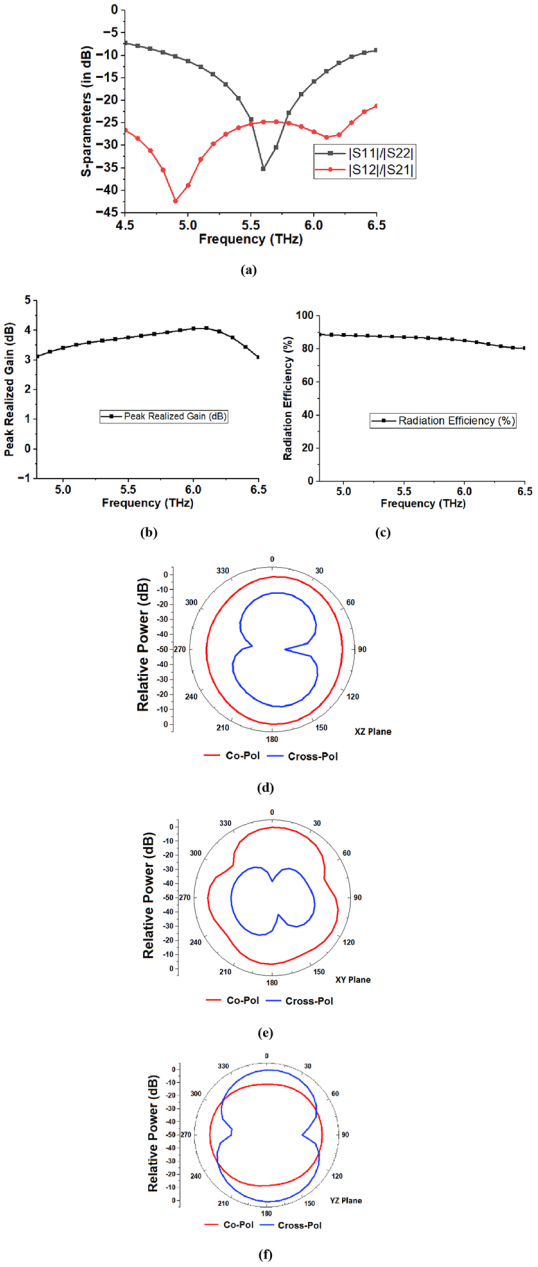

Fig. 5 Graphene loaded two-port antenna results. **a** S-parameters. **b** Gain. **c** Efficiency, radiation patterns in **d** xz plane **e** xy plane **f** yz plane

by the extreme rate of the transmission for trustworthy communication and the CCL value should not be higher than 0.4 bits/S/Hz. The CCL is calculated from the Eq. (12) where ψ^R is the correlation matrix.The CCL of the two-port antenna is not more than 0.4 bits/s/Hz which viewing the diverse characteristics of the antenna. The comparative analysis of the SRR-loaded antenna with the existing works is illustrated in the Table 2. The (Saxena

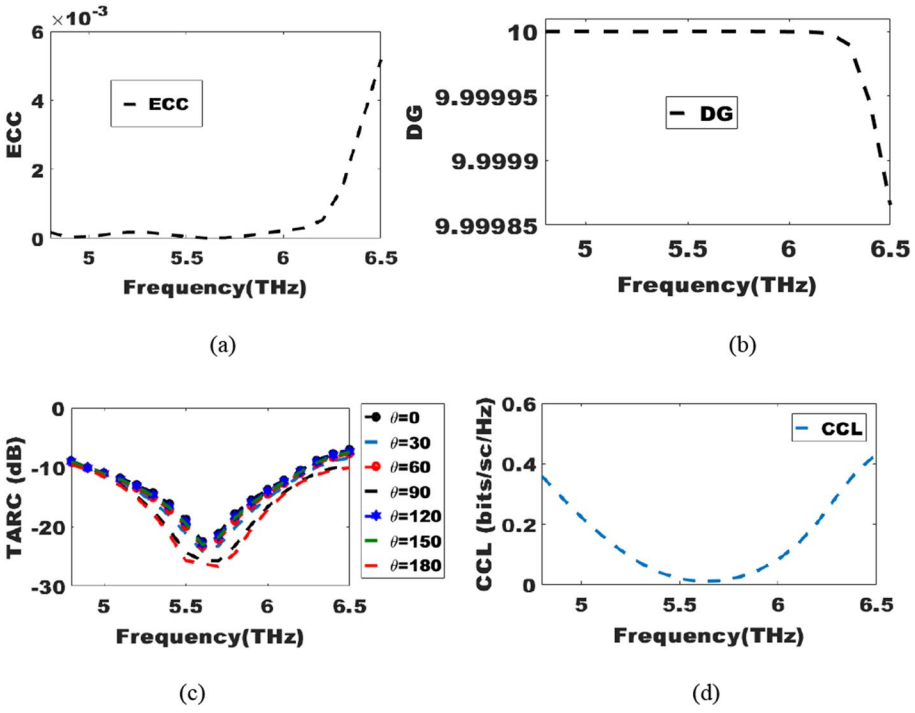

Fig. 6 MIMO characteristics **a** ECC **b** DG **c** TARC **d** CCL

et al. 2020; Keshwala 2021; Vasu Babu and Das 2022; Rubani et al. 2020; Prabhu and Malarvizhi 2022; Das et al. 2022; Singh and Varshney 2023) works are used large size of the antenna to improve the high isolation compared to proposed antenna. The (Maurya et al. 2023) used graphene based tuning model based on the bandstop Filter for isolation enhancement. The (Okan 2021; Vijayalakshmi et al. 2021; Singh and Varshney 2023) achieved less than 20 dB isolation where (Keshwala 2021; Vasu Babu and Das 2022; Okan 2021) are used unconnected ground. The proposed antenna which is compact and based on polarization diversity achieved more than 24.8 dB isolation can be efficiently work on THz applications.

$$ECC = \frac{\left|S_{11}^{*}S_{12} + S_{21}^{*}S_{22}\right|^{2}}{\left(1 - \left|S_{11}\right|^{2} - \left|S_{21}\right|^{2}\right)\left(1 - \left|S_{22}\right|^{2} - \left|S_{12}\right|^{2}\right)} \tag{8}$$

$$DG = 10\sqrt{1 - |ECC|^{2}} \tag{9}$$

$$TARC = \frac{\sqrt{\sum_{i=1}^{N}\left|b_i\right|^{2}}}{\sqrt{\sum_{i=1}^{N}\left|a_i\right|^{2}}} \tag{10}$$

Table 2 Comparative study of the SRR loaded two-port antenna for THz Applications

References	Substrate material	Size of the antenna μm × μm (λc × λc), where λc is the center frequency	|S11| in dB (THz)	Fractional bandwidth (%)	Isolation (dB)	Decoupling technology
Proposed	Silicon dioxide	30 × 30 (0.49λc × 0.49λc)	4.9 to 6.3	25	> 24.8	Tunable Graphene SRR and Diagonal Stub
Saxena et al. (2020)	RT5880	1400 × 1000 (24.10λc × 17.21λc)	0.33–10	187.22	> 30	Inverted L-shaped strip
Keshwala (2021)	Polyimide	100 × 180 (7.22λc × 12.96λc)	5.64–37.56	147.77	> 20	Unconnected Ground
Maurya et al. (2023)	Silicon dioxide	40 × 20 (0.81λc × 0.40λc)	5.68–6.51	13.61	> 20	Graphene based decoupling
Vasu Babu and Das (2022)	Polyimide	600 × 300 (0.98λc × 0.49λc)	0.276–0.711	88.14	> 20	Unconnected Ground
Okan (2021)	Rogers RO4835-T	2000 × 1000 (λc × 0.5λc)	0.095–0.205	73.33	> 17	Unconnected Ground
Rubani et al. (2020)	RT/Duriod/6010	36 × 35 (318λc x309λc)	8.84	–	> 22	Distance between antenna
Prabhu and Malarvizhi (2022)	Polyimide	1400 × 750 (1.4λc × 0.75λc)	0.3 and 10	–	> 20	Stubs and slot in ground
Vijayalakshmi et al. (2021)	Polyimide	50 × 40 (0.38λc × 0.30λc)	2.3, 3.2 and 4.5	–	> 15	Parasitic Strip
Das et al. (2022)	silicon dioxide	180 × 90 (1.37λc × 0.68λc)	1.6 to 3.0	60.1	> 20	Graphene loaded on patch and t-shaped stub
Singh and Varshney (2023)	silicon dioxide	100 × 150 (1.64λc × 2.46λc)	4.93 and 5.43	–	> 18.65	Graphene and multiple slots
Aghamohammadi et al. (2022)	Arion AD 250C	340 × 380 (0.66λc × 0.74λc)	0.55 to 0.63	13.53	> 23	Metamaterials
Saxena et al. (2022)	Quartz	960 × 480 (3.84λc × 1.92λc)	0.4 to 2.0	133.33	> 20	Metasurface

$$TARC = \frac{\sqrt{(\left|S_{11} + S_{12}e^{j\theta}\right|^2 + \left|S_{22}e^{j\theta} + S_{21}\right|^2)}}{\sqrt{2}} \tag{11}$$

$$CCL = -\log_2 \det\left(\psi^R\right) \tag{12}$$

6 Conclusion

The graphene based SRR-loaded on two-port antenna is discussed for the THz applications. The size of the antenna is compact the s-parameters can be tuned with the different chemical potentials of SRR. The two-port antenna works from 4.9 to 6.3 THz where the quadrupole mode of the SRR is used to obtain the maximum isolation of 42.3 dB when the distance of edges of the antenna is only $0.15\lambda_0$.The MIMO characteristics as ECC and CCL of the antenna validate the diversity performance and placement of the antenna to achieve the polarization diversity.

Author contributions Anubhav Kumar completed the simulation, experiment and validation of the antenna, Divya saxena completed the mathematics analysis and EC Model. Anubhav Kumar and Divya Saxena author wrote and reviewed the manuscript.

Funding Not applicable.

Availability of data and materials Not applicable.

Declarations

Competing interests The authors declare no competing interests.

Ethical approval Not applicable.

References

Aghamohammadi, M.H., Jarchi, S., Zamani, A.: Mutual coupling reduction in multiple-input multiple-output antenna based on metamaterial at low THz frequency band. In: 2022 6th International Conference on Millimeter-Wave and Terahertz Technologies (MMWaTT). IEEE (2022)

Akyildiz, I.F., Han, C., Nie, S.: Combating the distance problem in the millimeter wave and terahertz frequency bands. IEEE Commun. Mag. **56**(6), 102–108 (2018)

Ali, M.F., et al.: Terahertz antenna with controllable and tunable filtering characteristics. Micro Nanostruct. **174**, 207476 (2023)

Balanis, C.A.: Antenna Theory: Analysis and Design. Wiley (2015)

Dash, S., Patnaik, A.: Impact of silicon-based substrates on graphene THz antenna. Physica E **126**, 114479 (2021)

Das, P., Singh, A.K., Mandal, K.: Metamaterial loaded highly isolated tunable polarisation diversity MIMO antennas for THz applications. Opt. Quantum Electron. **54**(4), 250 (2002)

Gao, M., Li, K., Kong, F., Zhuang, H., Zhu, G.: Graphene-based composite right/left-handed leaky-wave antenna at terahertz. Plasmonics **15**, 1199–1204 (2020)

Hwu, S.U., deSilva, K.B., Jih, C.T.: Terahertz (THz) wireless systems for space applications. In: 2013 IEEE Sensors Applications Symposium Proceedings, pp. 171–175. IEEE (2013)

Kaipa, C.S., Yakovlev, A.B., Hanson, G.W., Padooru, Y.R., Medina, F., Mesa, F.: Enhanced transmission with a graphene-dielectric microstructure at low-terahertz frequencies. Phys. Rev. B **85**(24), 245407 (2012)

Keshwala, U.: Microstrip line fed sinusoidal tapered square shaped MIMO antenna for THz applications. Optik **247**, 167905 (2021)

Kiani, N., Hamedani, F.T., Rezaei, P.: Implementation of a reconfigurable miniaturized graphene-based SIW antenna for THz applications. Micro Nanostruct. **169**, 207365 (2022b)

Kiani, N., Hamedani, F.T., Rezaei, P.: Realization of polarization adjusting in reconfigurable graphene-based microstrip antenna by adding leaf-shaped patch. Micro Nanostruct. **168**, 207322 (2022a)

Kiani, N., Hamedani, F.T., Rezaei, P.: Reconfigurable graphene-gold-based microstrip patch antenna: RHCP to LHCP. Micro Nanostruct. **175**, 207509 (2023)

Kumar, A., Saxena, D.: Compact UWB microstrip antenna for THz communication application. In: 2020 9th International Conference System Modeling and Advancement in Research Trends (SMART), pp. 388–391. IEEE (2020)

Maurya, N.K., et al.: Graphene-based frequency agile isolation enhancement mechanism for MIMO antenna interahertz regime. Nano Commun. Netw. **35**, 100436 (2023)

Nickpay, M.R., Danaie, M., Shahzadi, A.: A wideband and polarization-insensitive graphene-based metamaterial absorber. Superlattices Microstruct. **150**, 106786 (2021)

Nickpay, M.-R., Danaie, M., Shahzadi, A.: Graphene-based metamaterial absorber for refractive index sensing applications in terahertz band. Diam. Relat. Mater. **130**, 109539 (2022a)

Nickpay, M.-R., Danaie, M., Shahzadi, A.: Design of a graphene-based multi-band metamaterial perfect absorber in THz frequency region for refractive index sensing. Physica E **138**, 115114 (2022b)

Nickpay, M.-R., Danaie, M., Shahzadi, A.: Wideband rectangular double-ring nanoribbon graphene-based antenna for terahertz communications. IETE J. Res. **68**(3), 1625–1634 (2022c)

Nickpay, M.-R., Danaie, M., Shahzadi, A.: Highly sensitive THz refractive index sensor based on folded split-ring metamaterial graphene resonators. Plasmonics. **17**, 237–248 (2022d)

Nickpay, M.-R., Danaie, M., Shahzadi, A.: A triple-band metamaterial graphene-based absorber using rotated split-ring resonators for THz biomedical sensing. Opt. Quant. Electron. **55**(2), 193 (2023a)

Nickpay, M.-R., Danaie, M., Shahzadi, A.: Graphene-based tunable quad-band fan-shaped split-ring metamaterial absorber and refractive index sensor for THz spectrum. Micro Nanostruct. **173**, 207473 (2023b)

Okan, T.: High efficiency unslotted ultra-wideband microstrip antenna for sub-terahertz short range wireless communication systems. Optik **242**, 166859 (2021)

Prabhu, P., Malarvizhi, S.: Koch fractal loaded high gain super-wideband diversity THz MIMO antenna for vehicular communication. Opt. Quantum Electron. **54**(11), 726 (2022)

Qi, L., Liu, C., Shah, S.M.A.: A broad dual-band switchable graphene-based terahertz metamaterial absorber. Carbon **153**, 179–188 (2019)

Rubani, Q., Gupta, S.H., Rajawat, A.: A compact MIMO antenna for WBAN operating at Terahertz frequency. Optik **207**, 164447 (2020)

Saxena, G., Awasthi, Y.K., Jain, P.: High isolation and high gain super-wideband (0.33–10 THz) MIMO antenna for THz applications. Optik **223**, 165335 (2020)

Saxena, G., Chintakindi, S., Kasim, M.A., Maduri, P.K., Awasthi, Y.K., Kumar, S., Dewan, C.: Metasurface inspired wideband high isolation THz MIMO antenna for nano communication including 6G applications and liquid sensors. Nano Commun. Netw. **34**, 100421 (2022)

Singh, R., Varshney, G.: Isolation enhancement technique in a dual-band THz MIMO antenna with single radiator. Opt. Quant. Electron. **55**(6), 539 (2023)

Sorathiya, V., Lavadiya, S., Parmar, B., Das, S., Krishna, M., Faragallah, O.S., Rashed, A.N.Z.: Numerical investigation of the tunable polarizer using gold array and graphene metamaterial structure for an infrared frequency range. Appl. Phys. B **128**, 1–9 (2022)

Torabi, E.S., Fallahi, A., Yahaghi, A.: Evolutionary optimization of graphene-metal metasurfaces for tunable broadband terahertz absorption. IEEE Trans. Antennas Propag. **65**(3), 1464–1467 (2017)

Varshney, G., et al.: Proximity-coupled two-port multi-input-multi-output graphene antenna with pattern diversity for THz applications. Nano Commun. Netw. **21**, 100246 (2019)

Vasu Babu, K., Das, S., Varshney, G., Jyothi Sree, G.N., Madhav, B.T.P.: A micro-scaled graphene-based tree-shaped wideband printed MIMO antenna for terahertz applications. J. Comput. Electron. **21**(1), 289–303 (2022)

Vijayalakshmi, K., KanimozhiSelvi, C.S., Sapna, B.: "Novel tri-band series fed microstrip antenna array for THz MIMO communications. Opt. Quantum Electron. **53**, 1–13 (2021)

Vishwanath, B.R., Sharma, V., Sahana, B.C., Varshney, G.: Controlling the resonant modes/bandwidth using graphene strip and isolation enhancement in a two-port THz MIMO DRA. Opt. Quantum Electron. **55**(7), 659 (2023)
Wang, X., He, X., Jiang, J., Yao, Y., Lu, G.: Programmable manipulation of terahertz beams by hybrid graphene-metal coding metasurfaces. Diam. Relat. Mater. **129**, 109378 (2022)
Woolard, D.L., Brown, R., Pepper, M., Kemp, M.: Terahertz frequency sensing and imaging: a time of reckoning future applications? Proc. IEEE **93**(10), 1722–1743 (2005)